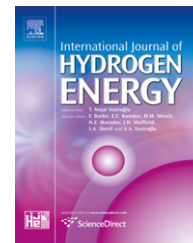


Available at www.sciencedirect.comjournal homepage: www.elsevier.com/locate/he

Size-resolved kinetics of Zn nanocrystal hydrolysis for hydrogen generation

Xiaofei Ma, Michael R. Zachariah*

Department of Mechanical Engineering and Department of Chemistry and Biochemistry, University of Maryland, College Park, MD 20742, USA

ARTICLE INFO

Article history:

Received 28 October 2009

Received in revised form

4 January 2010

Accepted 6 January 2010

Available online 29 January 2010

Keywords:

Hydrolysis

Kinetics

Zinc

Nanocrystal

Hydrogen energy

Ion-mobility

ABSTRACT

The substrate-free hydrolysis of Zn nanocrystals was investigated as the second step in a ZnO/Zn solar water-splitting thermochemical cycle. In this work, we combined two different ion-mobility schemes in series to study the hydrolysis kinetics of size-selected zinc nanocrystals (NCs). The first mobility characterization size selects particles with a differential mobility analyzer (DMA). The second mobility characterization employs an aerosol particle mass analyzer (APM) and measures changes in mass resulting from a controlled hydrolysis of the Zn NCs. A low temperature reaction mechanism is proposed to explain the mass change behavior of Zn NCs hydrolysis at 100–250 °C. An Arrhenius law was used to extract the reaction kinetic parameters. The hydrolysis activation energy and the order of the reaction with respect to water mole fraction were found to be 24 ± 2 kJ/mol and 0.9 ± 0.1 , respectively. Complete conversion of 70 nm Zn NCs was achieved at 175 °C with a residence time of about 10 s and water vapor mole fraction of 19%.

© 2010 Professor T. Nejat Veziroglu. Published by Elsevier Ltd. All rights reserved.

1. Introduction

Water-splitting thermochemical cycles have been demonstrated to bypass the H₂/O₂ separation problem which impedes single-step thermal dissociation of water, and further allows operation at relatively moderate upper temperatures [1]. Abraham [2] investigated the potential for water-splitting cycles based on general thermodynamic principles and concluded that the minimum number of reaction steps operating between 1000 K and 298 K is three. Previous studies were mostly focused on multistep thermochemical cycles using nuclear heat and were forced to operate under the temperature limit of about 1200 K [3]. However, these multiple steps (more than two) suffer from inherent inefficiencies associated with heat transfer and product separation at each step [1]. Two-step water-splitting cycles based on metal oxide redox pairs are

thermodynamically more efficient and can be achieved using concentrated solar energy. These type of cycles were first proposed by Nakamura [4] based on Fe₃O₄/FeO redox pair. In the first step of the cycle, solar energy is used to dissociate the metal oxide to metal or lower valence metal oxide. In the second step, metal is oxidized by water at moderate temperatures to form hydrogen and the corresponding metal oxide.

Among the feasible two-step water-splitting thermochemical cycles, the ZnO/Zn redox pair has attracted particular interest for its potential of achieving high energy conversion efficiency [5]. The theoretical upper limit is 44% with complete heat recovery. Several studies have been conducted on different aspects of the thermal dissociation of ZnO, and experimental solar furnace/reactors have been built for exploratory tests [6–13]. Our special interest in this paper focuses on the 2nd step of the ZnO/Zn cycle, the Zn hydrolysis

* Corresponding author. Tel.: +1 301 405 4311; fax: +1 301 314 9477.

E-mail address: mrz@umd.edu (M.R. Zachariah).

0360-3199/\$ – see front matter © 2010 Professor T. Nejat Veziroglu. Published by Elsevier Ltd. All rights reserved.

doi:10.1016/j.ijhydene.2010.01.011

reaction. The reaction is thermodynamically favorable below about 1400 K but with kinetic constraints [14]. The Zn hydrolysis reaction has been studied on various forms of Zn material such as Zn discs [15], liquid zinc [7,16], Zn vapor [17,18], Zn powder/nanoparticles [14,19–21] and on solar zinc [22,23]. Various analytic tools have been employed to probe the reaction kinetics and characterize the reaction products. For example, GC/MS has been used for hydrogen measurement, thermogravimetric analysis for monitoring reactant weight and X-ray, TEM and DMA for Zn/ZnO particle characterization. The reaction rate has been studied on Zn discs by Bazan et al. [15] at 21–50 °C, on liquid Zn by Bermann and Epstein [16] in the temperature range of 450–500 °C and on zinc powder by Funke et al. [24]. Clarke and Fray investigated the Zn hydrolysis reaction by analyzing the wall deposit in an aerosol reactor at a temperature up to 900 °C. The detailed experimental conditions and results from previous studies are summarized in Table 1.

More recently, researchers at ETH proposed using Zn nanoparticles for the hydrolysis reaction. Due to large surface to volume ratio of nanoparticles, the application of those materials should promote the reaction kinetics, heat and mass transfer, and thus favor complete or nearly complete reaction. Ernst [19] et al. at ETH using thermogravimetric analysis measured the reaction rate of Zn particles at the temperature region just below the Zn melting point. A core-shell model was used to quantify the hydrolysis rate. However, conventional systems such as TGA are known to be corrupted by heat and mass transfer effects which greatly influences the accuracy of kinetics obtained by these methods [25,26]. Furthermore, using nanoparticles with a wide size distribution makes extraction of accurate kinetics difficult. To deal with the two issues outlined above we employ an on-line tandem ion-mobility method which allows us to determine the intrinsic hydrolysis kinetics of in-situ generated unsupported Zn NCs by measuring the mass change of a single particle of precisely known size.

In this study, we focused on the reaction kinetics of Zn NCs hydrolysis at relatively low temperatures (100–250 °C). From a practical point of view a lower reaction temperature is desirable from efficiency and materials engineering standpoint. Furthermore, low temperatures enable one to bypass the material loss problem due to Zn evaporation. Our preliminary experiments of Zn hydrolysis in the temperature range of 100–250 °C have shown significant mass changes of Zn NCs. Some previous studies also show that hydrogen can be harvested by Zn hydrolysis at temperatures below 100 °C. For example, the theoretical and experimental work of Alimenti [27] and Bazan's [15] experiment on Zn disk prove that the hydrolysis reaction of bulk Zn can proceed at room temperature with the evolution of molecular hydrogen. Furthermore, studies of Zn corrosion in an outdoor atmosphere [28] primarily by moisture have indicated a measurable reaction rate of hydrolysis. According to Mattsson [29], the Zn corrosion rate under atmospheric exposure can be as high as 16 $\mu\text{m}/\text{year}$, which is about 2 nm/h [28].

2. Experiment setup

The experimental system consists of three components. Preparation of monodisperse Zn NCs, exposure of size-

selected Zn NCs into a controlled temperature region, and finally, measurement of the mass change resulting from hydrolysis. A complete schematic of the experimental system with temperature and flow rate control is shown in Fig. 1. Our experiment consists of two different ion-mobility schemes in series. The first mobility characterization is to size select NCs with a differential mobility analyzer (DMA) [30]. The second mobility characterization employs an aerosol particle mass analyzer (APM) and measures changes in mass resulting from a controlled hydrolysis of the Zn NCs.

Water vapor is generated by bubbling Ar gas at a flow rate of 0.5 LPM (liter per minute) through heated distilled water. In order to prevent any condensation of water vapor in the gas lines, the whole water injection system is wrapped with heating tapes and heated to ~ 70 °C. Two diffusion dryers are placed between the hydrolysis furnace and the APM sampling port to prevent water condensation in the instruments.

Since we are employing ion-mobility methods, particles are first charged to a Boltzmann charge distribution by exposing the nanoparticle aerosol to a Po-210 source, before the DMA. The average charge state of sample particles under Boltzmann distribution is quasi-neutral, with most of particles uncharged and equal amount of particles carry $+/-1$ charge and $+/-2$ charges, etc. For example, in case of 50 nm particles, 60.2% particles will be neutral, 19.3% carry $+/-1$ charge, 0.6% carry $+/-2$ charges, and higher charge state would be even less. Considering the small percentage in the multiple charged states, we ignore multiple charged particles. Both the DMA and APM are configured to classify positively charge particles for these experiments.

2.1. In-situ generation of monodisperse Zn NCs

The Zn NCs are generated using an evaporation/condensation method in argon. Granular Zn (purity, $\geq 99.99\%$ from Sigma-Aldrich) contained in a small ceramic boat was placed in a tube furnace at 550 °C to generate a flow of Zn vapor. The Zn vapor condenses as it exits the tube furnace and by empirical adjustment of the tube furnace temperature, and the argon carrier gas flow rate we were able to form unagglomerated Zn NCs. Since our objective is to study size-resolved reactivity we use a DMA as a band pass filter to generate monodisperse NCs. The DMA selects size based on the electric mobility which is related to the drag force and charge on a particle.

2.2. The DMA-APM system

The DMA, used in this experiment for generating monodisperse NCs, consists of an annular region between two concentric cylinders, with the center cylinder held at high voltage and the outer one at ground. Charged particles of the right polarity feel an attractive force toward the center electrode and move radially inward at an electrophoretic velocity determined by the particle charge, and drag force which is a function of particle size. When charged particles flow between the cylinders the electric force on the particle is balanced by the drag force, and at a fixed voltage all particle exiting the instrument have (to the resolution of the instrument) equivalent mobility sizes. In the size range of consideration here, the DMA functions as a source of mono-area NCs.

Table 1 – Summary of recent studies on the Zn hydrolysis reaction.

Zn material	Temperature	Experimental tools	Reaction kinetics	Hydrogen conversion	Reference
solar Zn nanoparticle with void fraction of $91 \pm 1\%$	748–803 K	catharometric analyzer environmental SEM	activation energy of 87 ± 7 kJ/mol, and reaction order of 3.5 ± 0.5	maximum H ₂ yield ~55%	[23]
sub-micron Zn particles, dBET = 164 ± 10 nm	330–360 °C	thermogravimetric balance, TEM, XRD, GC	an initially linear conversion profile followed by a parabolic conversion profile independent of water mole fraction	maximum ZnO content ~95%, at 350 °C with reaction time ~180 min and water mole fraction of 0.4	[21]
Zn particles (average size 158 nm)	653–813 K	thermogravimetric analysis, TEM, SEM, EDS, combustion oxygen analyzer	activation energy of 132 ± 27 kJ/mol	maximum 24% at 813 K with residence time of 0.6 s	[24]
in-situ formation and hydrolysis of Zn aerosol	1023 K and 1073 K	GC, X-ray, TEM, DMA	Zn vapor deposition followed by heterogeneous reaction on the wall	87–96% at residence time 1.71 and 2.12 min	[18]
solar Zn powder	458–833 K	hydrogen analyzer, X-ray, TEM	two stages observed, reactivity is higher for solar Zn powder than for commercial Zn	24–81% for temperature range 458–833 K	[22]
in-situ formation and hydrolysis of Zn aerosol	573–1273 K	thermogravimetric analysis, GC, TEM	H ₂ formation is favored by heterogeneous reaction, higher reaction temperature.	up to 90% H ₂ conversion at T _R > 900 K	[19]
in-situ formation and hydrolysis of Zn aerosol	923, 1023 and 1073 K	GC, X-ray, TEM	conversion reaches optimum at 1023 K, ZnO passivating layer on larger particles is the reaction barrier	37–72% at 923 and 1023 K and decrease to 37% at 1073 K	[20]
in-situ formation and hydrolysis of Zn nanoparticles	1023 K and 1073 K	GC, X-ray	two reaction mechanisms, (1) reaction of Zn(g) and stream at reactor wall (2) reaction between Zn(l) or Zn(s) and stream at particle Surface	average of 60% and 45% at 1023 K and 1073 K	[14]
liquid Zn	723–773 K	GC	Diffusion through ZnO is the rate determining step. The order of reaction is $0 < n < 1$. Kinetic expression is $W_{sp} = kP_{H_2O}/(1 + bP_{H_2O})$		[16]
commercial Zn (mean size of 10 μm) and solar Zn (mean size of 9 μm)	623–773 K	thermogravimetric analysis	reaction proceeds faster for molten Zn and Zn containing impurities	Zn content >50% for commercial. Zn content <10% for solar Zn	[17]

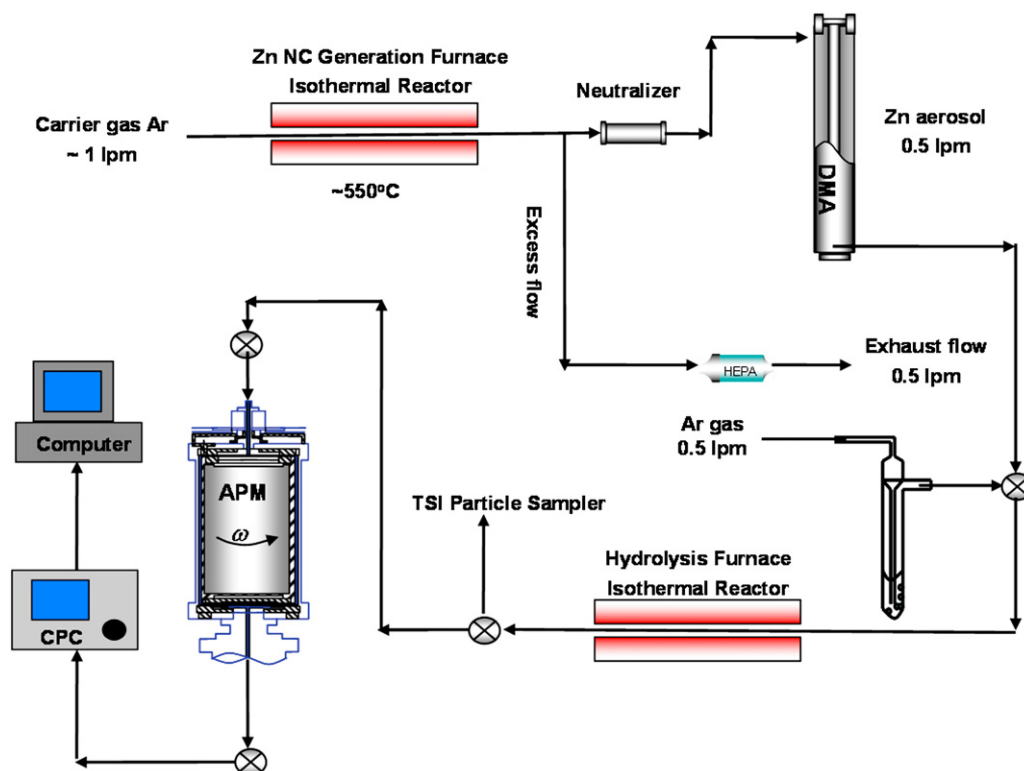


Fig. 1 – Experimental system for Zn, generation, size-selection by DMA, hydrolysis and subsequent mass analysis with the APM.

The APM can determine the particle mass distribution based on particle mass to charge ratio, and is used in our experiment to monitor changes to the particle mass resulting from oxidation. The APM consists of two concentric cylindrical electrodes that rotate together at a controlled speed. An electrical field is created by applying high voltage on the inner electrode while the outer one is held at ground. Charged particles flowing within the concentric cylinders experience opposing centrifugal and electrostatic forces and as a result particles exiting the instrument at fixed voltage and rotation speed all have the same nominal mass. By scanning either the voltage or the rotation speed, the particle mass distribution (independent of particle shape) can be determined. APM mass measurements are independent of particle morphology because the centrifugal force is directly proportional to the mass. The DMA-APM techniques employed here allows for a direct measure of mass change of individual particles, and thus enables us to explore the intrinsic reactivity of NCs while minimizing the sampling error introduced by mass and heat transfer inherent in bulk power samples. Our previous experiments have used the DMA-APM technique to measure the inherent density of nanoparticles, as well as to study the mechanism of aluminum, nickel and zinc oxidation [30–32].

Based on operating conditions for the DMA and APM, we estimate uncertainties as follows. For the DMA operating conditions the uncertainty is based on the theoretical transfer function which will give an uncertainty in the peak particle size of $\pm 4\%$. We then use Gaussian fit to determine the peak size which would have a precision uncertainty of no more than 1%. A similar result can be obtained for the APM however

the uncertainties are not due to the transfer function but uncertainties in the step voltage which has a resolution of only ± 0.5 V, which gives an uncertainty in mass of $\sim 4\%$. Using the root-sum-square (RSS) method, we can estimate the uncertainty of density calculation $\sim 5\%$. This is consistent with prior work using combined DMA/APM on reference aerosols (NaCl and DOP) which gave an experimentally determined uncertainty in density of 4% [33].

Furthermore, our DMA/APM mass measurements of NIST SRM[®] 60 and 100 PSL spheres were within about 1.4% and 5.6%, respectively [34].

2.3. Zinc nanocrystals characterization, sampling and hydrolysis

In our experiment, Zn NCs of initial ion-mobility size of 70 nm were selected to study the hydrolysis reaction. After size classification, the Zn aerosol flow is mixed with Ar gas (carrying water vapor) at the ratio of 1:1 and then passes through a second tube furnace. This furnace enables the controlled hydrolysis of the Zn NCs. The total flow rate of the aerosol flow is 1 LPM at STP. The Zn particle concentration after the DMA size-selection is about 3000 per cm^3 and the Zn mass concentration in the hydrolysis furnace is about 4E-12 g/cc, assuming the particles are 70 nm spherical particles and the density of Zn is 7.14 g/cc. At these particle densities no particle–particle interactions are expected to occur in the time scale of the experiment and any exothermicity in the reaction is both insufficient to either heat the particle or the ambient gas temperature. To monitor the small mass change of the NCs

due to hydrolysis, an aerosol particle mass analyzer (APM) is placed downstream. Particles exiting the APM will be selected on the basis of mass and are counted using a standard particle counting method, condensation particle counter (CPC).

In the experiment, the temperature in the hydrolysis furnace was set between 100 and 250 °C in increments of 25 °C. The particle mass distribution was then measured for each furnace temperature after the system reached steady state. The room temperature particle mass distribution was also taken, and set as the base of the mass measurement. Samples for electron-microscopic analysis were collected exiting the evaporation furnace by electrostatically precipitating the aerosol onto a TEM grid.

3. Results and discussion

3.1. Zn nanocrystal morphology

Fig. 2 shows the SEM image of two single Zn NCs that were deposited from the gas phase by electrostatic precipitation onto a TEM grid before size-selection. The NCs show the shape of near perfect hexagonal-prisms. Energy dispersive X-ray (EDS) spectra obtained from the NCs in SEM confirmed that the composition is Zn. Selected Area Electron Diffraction analysis indicated that the Zn NCs have top surfaces of {0001} crystal planes and have side surfaces of {1100} planes.

3.2. Zn nanocrystal mass measurement

Fig. 3 shows the normalized particle mass distributions for 70 nm mobility size Zn NCs reacting with water vapor at different temperatures. Fig. 3(a) and (b) are corresponding to a water vapor fraction of 3% while Fig. 3(c) and (d) are for the water vapor fraction of 15%. In each plot, the particle number concentration is plotted against the particle mass. These distributions are obtained from APM-CPC measurements. The particle number concentration is obtained with a condensation particle counter (CPC) while changing the APM voltage. Each data point in Fig. 3 is a time average of ~1 min of CPC counts in

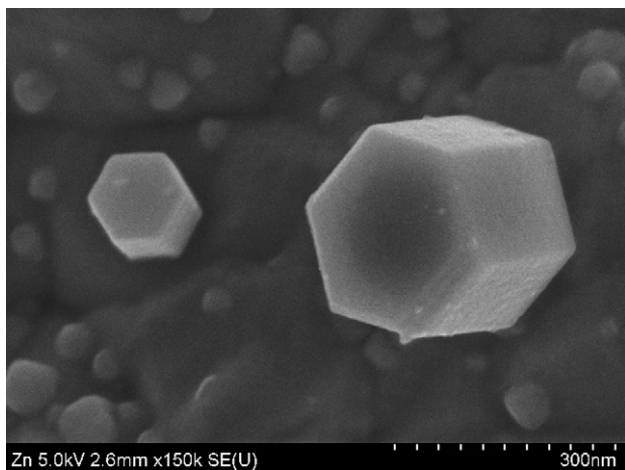


Fig. 2 – SEM image of the hexagonal-prism-shaped Zn NCs (before size-selection).

order to minimize the effect of system instability. The peak mass of Zn NCs at each hydrolysis temperature is obtained by fitting the experimental data using a Gaussian distribution. From Fig. 3(a) and (c), we can see that as we increase the hydrolysis temperature, the particle mass distributions shift to the larger mass side, which indicates that Zn NCs gain weight by reacting with water. However, upon further increase in the reaction temperature, the particle masses decrease as can be seen from Fig. 3(b) and (d). Similar trends of mass change has also been observed for 100 nm Zn NCs. Fig. 4 displays the plots of Zn NC mass as a function of reaction temperature for 70 nm Zn NCs based on the results of particle mass measurement. Also shown in these plots is the residence time corresponding to each hydrolysis temperature. The residence time is determined using the following equation:

$$\tau = \int_0^L \frac{1}{u(x)} dx \quad (1)$$

where L is the length of the tube and $u(x)$ is the flow velocity, which can be calculated below as:

$$u(x) = \frac{4}{3} u_m \frac{T(x)}{T_0} \quad (2)$$

where $4/3 u_m$ is the peak flow velocity of carrier gas calculated from volumetric flow rate and the cross sectional area of the flow tube under the assumption of laminar flow. $T(x)$ is temperature profile within the tube at each furnace set point.

3.3. Low temperature Zn hydrolysis reaction mechanism

Based on the mass change behavior of Zn NCs during hydrolysis as a function of temperature, we proposed the following reaction mechanism:

At relatively low temperature (below 150 °C) Zn NCs can react with water and generates solid zinc hydroxide and releases hydrogen gas. The reaction proceeds as follows:



Since zinc hydroxide ($\text{Zn}(\text{OH})_2$) has a low decomposition temperature (there is a range of reported $\text{Zn}(\text{OH})_2$ decomposition temperature from 125 °C to 196 °C), higher temperatures lead to zinc hydroxide decomposition via:



which competes with the hydrolysis reaction (3) and form ZnO. Thus, the overall reaction at high temperatures becomes $\text{Zn} + \text{H}_2\text{O} \rightarrow \text{ZnO} + \text{H}_2$. Since ZnO has a smaller molecular weight than $\text{Zn}(\text{OH})_2$, the total mass of NCs begin to decrease as the temperature increases. The above reaction mechanism is consistent with the reduction in mass as the temperature was increased. Our proposed mechanism is also supported by the following evidence:

First, both experimental and theoretical works [27,35] studying ZnO thin film formation using chemical vapor deposition have suggested that $\text{Zn}(\text{OH})_2$ can be easily formed in the hydrolysis reaction, but the formation of ZnO is very endothermic.

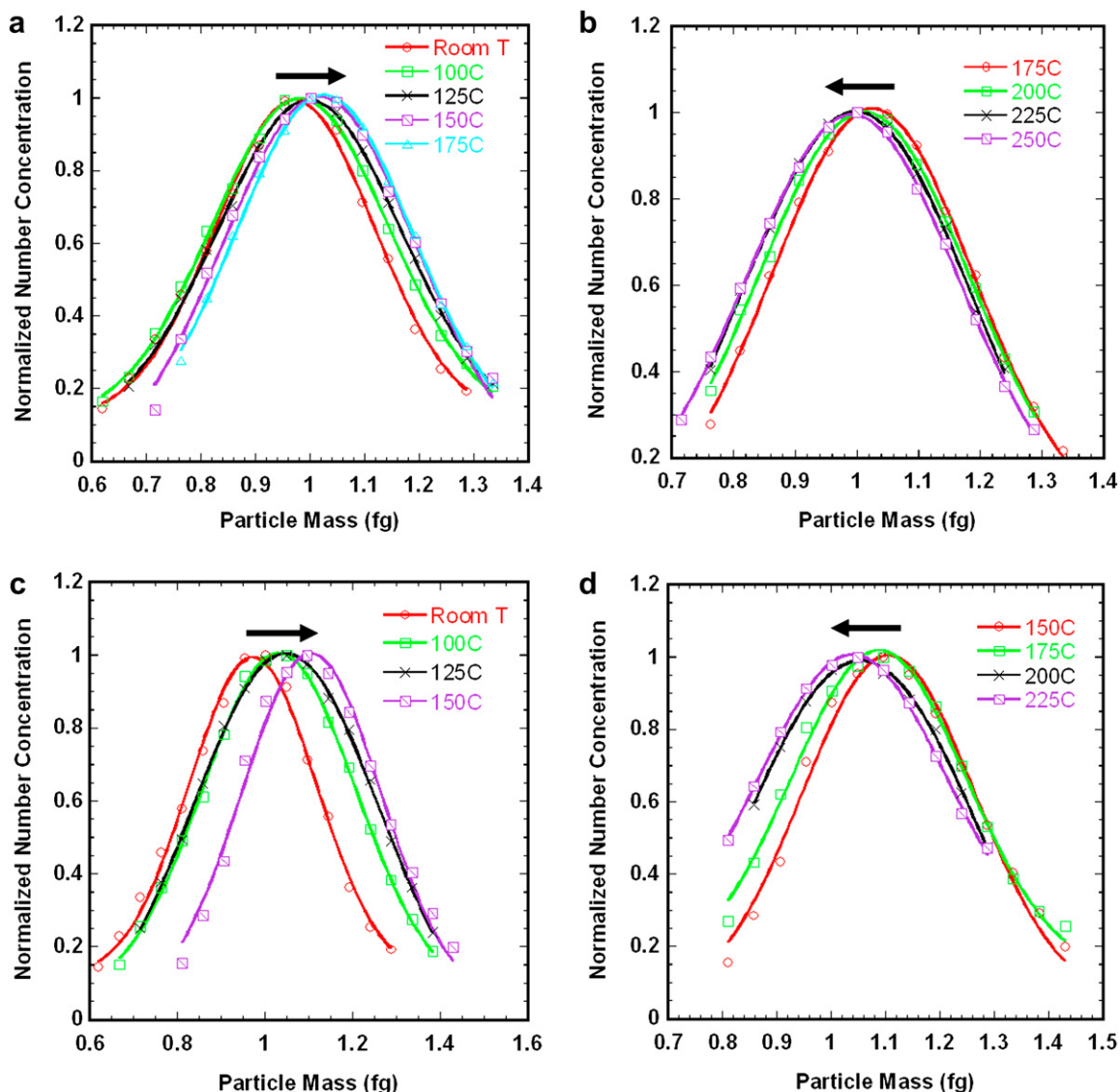


Fig. 3 – Normalized particle mass distributions for 70 nm mobility size Zn NC at different hydrolysis temperatures. Plots (a) and (b) are for the water vapor fraction of 3%. Plots (c) and (d) are for the water vapor fraction of 15%.

Second, zinc hydroxide is the principal constituents of the Zn corrosion layers resulting from exposure to natural environments [28].

Third, based on the results of Alimenti's theoretical modeling [27], when two water molecules were adsorbed onto Zn, the intermediary product was $\text{Zn}(\text{OH})_2 + \text{H}_2$ and the equilibrium state was $\text{ZnO} + \text{H}_2\text{O}$. In our aerosol experiment, water is by far the excess reactant.

However, it is also possible that the reaction product is ZnO with some chemisorbed water, $\text{ZnO} \times n\text{OH}$ as suggested by Bazan [15].

To further determine the product composition, Energy Dispersive X-ray (EDS) characterization was conducted on the hydrolyzed NCs. Fig. 5 shows the results of the (EDS) analysis of 70 nm Zn NCs after reaction with water vapor at 100 °C. The sample was collected by electrostatically precipitating the aerosol onto a TEM grid. The TEM image in Fig. 5 clearly shows that the hydrolyzed Zn NC exhibits a core-shell structure. The

EDS results indicate a higher concentration of elemental oxygen on the NC shell (hydrogen cannot be detected by EDS). The extremely low mass loading (of the order of femtogram) in an aerosol experiment prevents the usage of conventional material characterization method such as TGA and XRD which require milligrams of materials. To further verify the proposed reaction mechanism, a fixed-bed reactor configuration was employed with commercial Zn powders (Sigma-Aldrich, $\geq 99\%$, more than 95% of the particles are not larger than 45 nm). The reactor was a 3/8" ID, 25 cm long stainless tube filled with Zn powder and externally heated 100 °C. A carrier nitrogen gas flow of 3 sccm containing 15% mole fraction water vapor was passed through the Zn bed. After reacting with water vapor for ~ 30 min, the hydrolyzed Zn powder was harvested for TGA analysis.

Fig. 6 shows the TGA results of the hydrolyzed commercial Zn powder. From the figure, we can clearly see two plateaus in the sample mass curve. The first mass plateau was reached at about 90 °C when all the absorbed water in the sample was

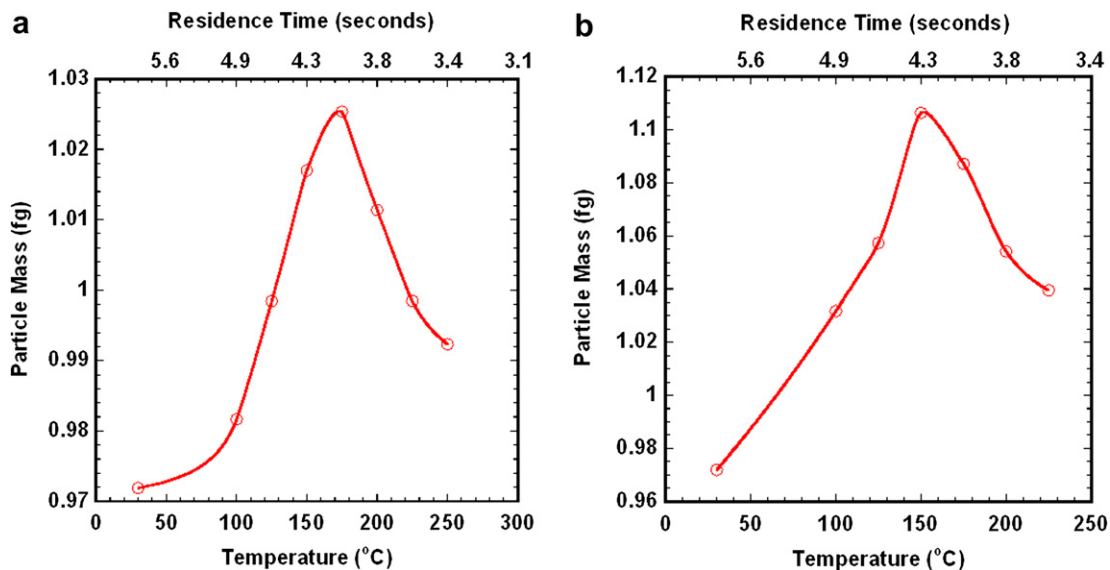


Fig. 4 – Particle mass vs. hydrolysis temperature for 70 nm Zn NCs. (a) 3% water vapor fraction (b) 15% water vapor fraction.

evaporated. As the TGA temperature was increased a second plateau is seen, which we believe is consistent with weight loss due to the decomposition of $\text{Zn}(\text{OH})_2$. The decomposition onset temperature is estimated from the TGA results to be $\sim 120^\circ\text{C}$. Further mass loss at higher temperatures is

associated with evaporation of the unreacted Zn (Ma X. et al. unpublished). Based on the mass difference between the two mass plateaus, we estimate the original percentage of conversion from Zn to $\text{Zn}(\text{OH})_2$ in the sample to be $\sim 36\%$. The TGA experiment confirms that $\text{Zn}(\text{OH})_2$ is formed during the

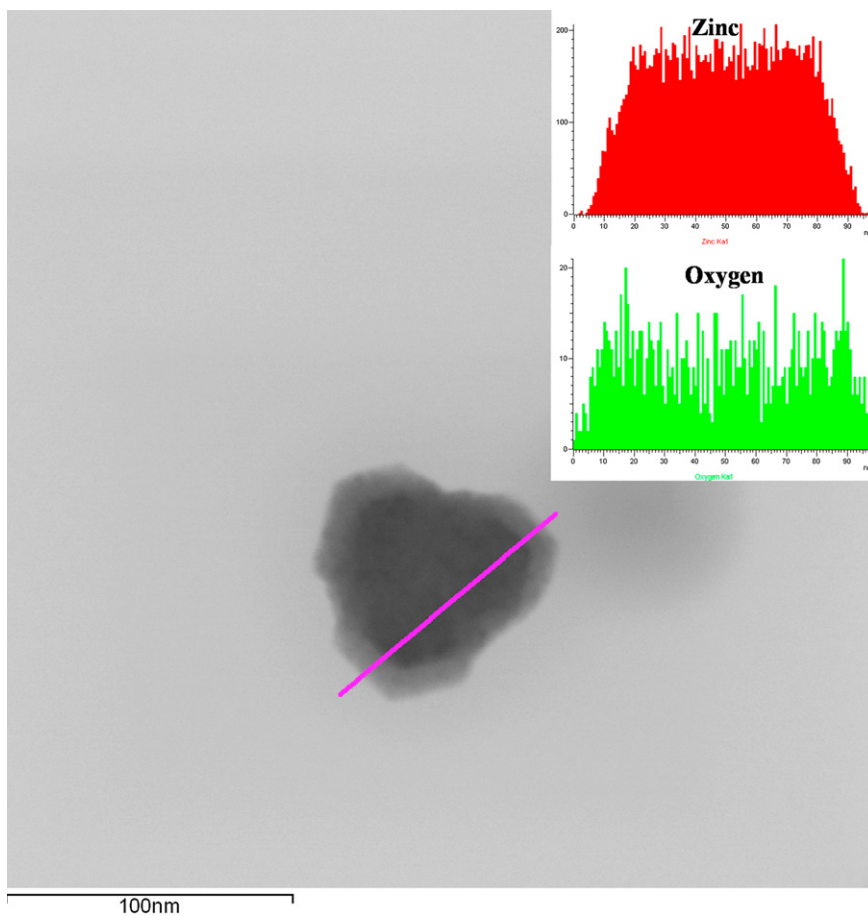


Fig. 5 – EDS analysis of a 70 nm Zn nanocrystal hydrolysis at 100 °C.

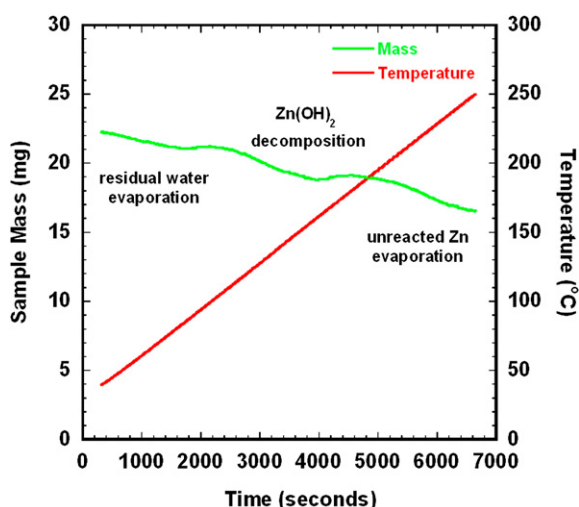


Fig. 6 – TGA measurement of the hydrolyzed commercial Zn powder reacted with water vapor at 100 °C for ~30 min.

hydrolysis of nano-sized Zn particles at temperature around 100 °C. To determine the gas products from Zn hydrolysis reaction in the fixed-bed reactor the reactor gas effluent was also sampled into a mass spectrometer (Stanford Research Systems, UGA 300). Hydrogen was observed during the hydrolysis of commercial Zn powder at 100 °C.

Based on the proposed hydrolysis mechanism, complete Zn to Zn(OH)₂ conversion has been achieved on the in-situ generated Zn NCs. Fig. 7 shows a particle mass distribution of 70 nm Zn NCs reacted with 19% mole fraction of water vapor at residence times of ~10 s. Based on the peak mass of Zn NCs, we can confirm that the 70 nm Zn NCs were fully converted into zinc hydroxide at the temperature of 175 °C. The inset in Fig. 7 shows the percentage of conversion as a function of

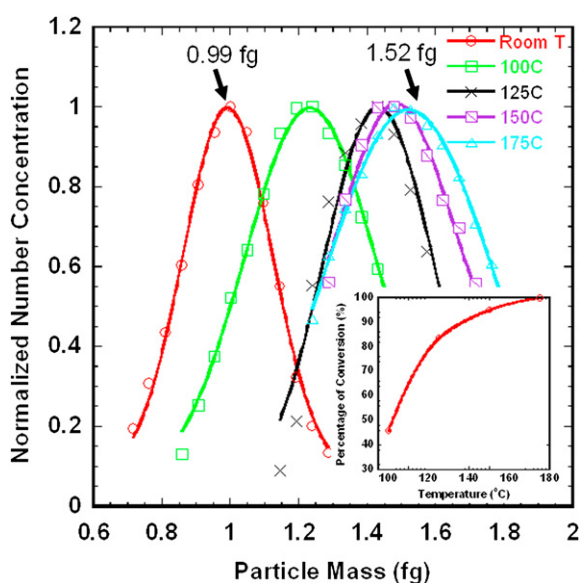


Fig. 7 – Particle mass distributions for 70 nm Zn nanocrystals reacting with 19% mole fraction of water vapor at different temperatures. (Inset) Percentage of conversion as a function of temperature.

furnace temperature. Compared with the hydrolysis of commercial Zn powder in the fixed-bed reactor, the hydrolysis of unsupported Zn NCs enjoys a much higher conversion rate. It is well known that bulk methods suffer from heat and mass transfer effects, milligrams of an aggregated sample are needed, while the sample mass of our aerosol based techniques is ~1 fg and is being performed on an isolated NC.

Compared with the overall hydrolysis reaction $\text{Zn} + \text{H}_2\text{O} \rightarrow \text{ZnO} + \text{H}_2$, the reaction (4) can proceed at lower temperatures and release hydrogen, which makes Zn hydrolysis more energy efficient and can bypass the material loss problem due to Zn evaporation at high temperatures.

3.4. Kinetics of the hydrolysis reaction

It is assumed that the reaction rate for Zn NC hydrolysis reaction follows an Arrhenius law. In our experiment, the reaction rate k are approximated by the average mass change rate $\frac{\Delta m}{\tau}$ (Δm is the mass difference measured by DMA-APM and τ is the residence time) of the NCs. The activation energy of the Zn hydrolysis can be extracted by plotting the reaction rate as a function of reaction temperature in an Arrhenius form. Fig. 8 shows the Arrhenius plots for 70 nm Zn NCs hydrolysis at different water mole fractions. The slopes of the straight lines are roughly equal to each other which suggests that we are measuring the same mechanistic process, and yield an overall activation energy of 24 ± 2 kJ/mol for the reaction (1). Previous studies on sub-micron Zn powders and nanoparticles showed strong discrepancies in the Zn hydrolysis activation energy, ranging from 132 kJ/mol [24] to 43 kJ/mol [21]. The big differences in activation energy can be explained by methods of preparation, initial oxide content and morphology of the reacting particles [23]. Those studies measured the activation energy based on the reaction $\text{Zn} + \text{H}_2\text{O} \rightarrow \text{ZnO} + \text{H}_2$. Unfortunately, no comparable kinetic data have been reported for the reaction $\text{Zn} + 2\text{H}_2\text{O} \rightarrow \text{Zn(OH)}_2 + \text{H}_2$ for which we can compare our studies on free Zn NC's.

Since the reaction rate depends strongly on the water vapor concentration, the experimental data are fitted to determine the

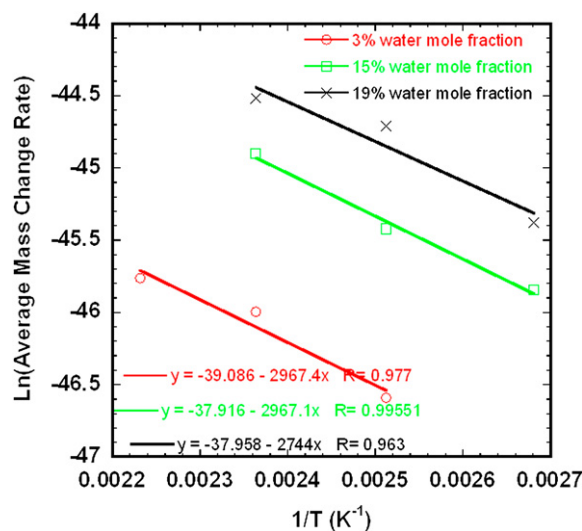


Fig. 8 – Arrhenius plot of the reaction rate for 70 nm Zn NCs hydrolysis at different water vapor concentrations.

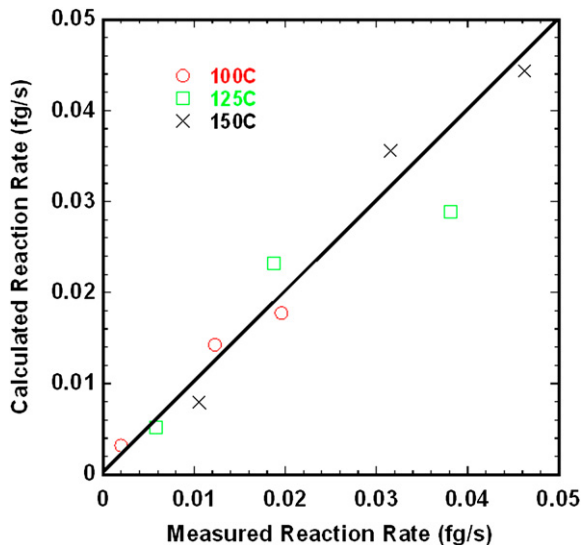


Fig. 9 – Calculated reaction rate based on equation (5) vs. measured reaction rate for 70 nm Zn NCs.

reaction order n with respect to the water vapor mole fraction y . The least square fit of the reaction rates yields a dependence of 0.91 ± 0.1 th order on the water vapor mole fraction and a pre-exponential factor A equals to $0.012 \text{ fg/nm}^2 \text{ s}$. Based on water vapor flux and the mass change rate of the NC an effective sticking coefficient of water molecules hitting Zn NCs was also calculated. This value is estimated to be between 10^{-7} to 10^{-6} in the temperature range investigated. A first order dependence on water concentration and a low value of effective sticking coefficient imply that the hydrolysis reaction is limited by the diffusion of water molecule or water fragment through the oxide layer and this diffusion depends on the water solubility on the NC surfaces. For comparison, Frank et al. [21] investigated the hydrolysis rate of Zn particles by up to 50 mol% water vapor at $330\text{--}360^\circ\text{C}$ and found a reaction order of 0.5th on water vapor mole fraction. Bazan et al. [15] studied the interaction between metallic zinc and water vapor and reported a 0.8th dependence on relative humidity in the temperature range $20\text{--}50^\circ\text{C}$.

To summarize, the overall kinetics of the hydrolysis reaction for 70 nm Zn NCs can be written as:

$$k = Ay^n \exp\left(-\frac{E_a}{RT}\right) \quad (5)$$

where $A = 0.012 \text{ fg/nm}^2 \text{ s}$ is the pre-exponential factor, $n = 0.9 \pm 0.1$ is the reaction order with respect to the water vapor mole fraction and $E_a = 24 \pm 2 \text{ kJ/mol}$ is the reaction activation energy. A comparison between of the experiment and the model of the reaction kinetics is shown in Fig. 9 in which the measured reaction rate is plot against the calculated reaction rate using equation (5). A good agreement is found over the entire experimental range.

4. Conclusions

In conclusion, we have successfully generated size-classified Zn NCs and have demonstrated that the hydrolysis kinetics of

free Zn NCs can be studied by an in-flight tandem DMA-APM method. Based on the mass change of Zn NCs, we proposed a low temperature reaction mechanism for Zn NC hydrolysis. At low temperatures (below 150°C) Zn NCs can react with water and generates solid zinc hydroxide and releases hydrogen gas. At higher temperatures, the zinc hydroxide decomposition reaction $\text{Zn(OH)}_2 \rightarrow \text{ZnO} + \text{H}_2\text{O}$ starts to competes with the hydrolysis reaction and form ZnO. This mechanism is consistent with the experiment observations and can produce hydrogen at the temperature range of about $100\text{--}150^\circ\text{C}$. Complete conversion of 70 nm Zn NC was achieved at 175°C with the residence time of 10 s and water vapor mole fraction of 19%. An Arrhenius law was used to extract the reaction kinetic parameters. The activation energy of the hydrolysis reaction for 70 nm Zn NCs is determined to be $24 \pm 2 \text{ kJ/mol}$ and the reaction order with respect to the water vapor mole fraction is found to be 0.9 ± 0.1 .

Acknowledgment

Support for this work comes from the National Science Foundation and University of Minnesota Initiative for Renewable Energy and the Environment. In addition, the authors wish to acknowledge the microscopy support through the University of Maryland Nanocenter and the University of Maryland NSF-MRSEC.

REFERENCES

- [1] Steinfeld A. Solar thermochemical production of hydrogen – a review. *Solar Energy* 2005;78(5):603–15.
- [2] Abraham BM, Schreine F. General principles underlying chemical cycles which thermally decompose water into elements. *Industrial and Engineering Chemistry Fundamentals* 1974;13(4):305–10.
- [3] Kodama T, Gokon N. Thermochemical cycles for high-temperature solar hydrogen production. *Chemical Reviews* 2007;107:4048–77.
- [4] Nakamura T. Hydrogen production from water utilizing solar heat at high-temperatures. *Solar Energy* 1977;19(5):467–75.
- [5] Steinfeld A. Solar hydrogen production via a two-step water-splitting thermochemical cycle based on Zn/ZnO redox reactions. *International Journal of Hydrogen Energy* 2002; 27(6):611–9.
- [6] Weidenkaff A, Steinfeld A, Wokaun A, Auer PO, Eichler B, Reller A. Direct solar thermal dissociation of zinc oxide: condensation and crystallisation of zinc in the presence of oxygen. *Solar Energy* 1999;65(1):59–69.
- [7] Weidenkaff A, Reller AW, Wokaun A, Steinfeld A. Thermogravimetric analysis of the ZnO/Zn water splitting cycle. *Thermochimica Acta* 2000;359(1):69–75.
- [8] Palumbo R, Lede J, Boutin O, Ricart EE, Steinfeld A, Moller S, et al. The production of Zn from ZnO in a high-temperature solar decomposition quench process – I. The scientific framework for the process. *Chemical Engineering Science* 1998;53(14):2503–17.
- [9] Moller S, Palumbo R. The development of a solar chemical reactor for the direct thermal dissociation of zinc oxide. *Journal of Solar Energy Engineering-Transactions of the Asme* 2001;123(2):83–90.

- [10] Moller S, Palumbo R. Solar thermal decomposition kinetics of ZnO in the temperature range 1950–2400 K. *Chemical Engineering Science* 2001;56(15):4505–15.
- [11] Schunk LO, Haerberling P, Wepf S, Wuillemin D, Meier A, Steinfeld A. A receiver-reactor for the solar thermal dissociation of zinc oxide. *Journal of Solar Energy Engineering-Transactions of the Asme* 2008;130(2).
- [12] Muller R, Lipinski W, Steinfeld A. Transient heat transfer in a directly-irradiated solar chemical reactor for the thermal dissociation of ZnO. *Applied Thermal Engineering* 2008;28(5–6):524–31.
- [13] Muller R, Steinfeld A. H₂O-splitting thermochemical cycle based on ZnO/Zn-redox: quenching the effluents from the ZnO dissociation. *Chemical Engineering Science* 2008;63(1):217–27.
- [14] Wegner K, Ly HC, Weiss RJ, Pratsinis SE, Steinfeld A. In situ formation and hydrolysis of Zn nanoparticles for H-2 production by the 2-step ZnO/Zn water-splitting thermochemical cycle. *International Journal of Hydrogen Energy* 2006;31(1):55–61.
- [15] Bazan JC, Gschaider ME, Alimenti GA. Gravimetric study of interaction of water vapour with metallic zinc. *Journal of Thermal Analysis and Calorimetry* 1999;55(2):569–79.
- [16] Berman A, Epstein M. The kinetics of hydrogen production in the oxidation of liquid zinc with water vapor. *International Journal of Hydrogen Energy* 2000;25(10):957–67.
- [17] Melchior T, Piatkowski N, Steinfeld A. H-2 production by steam-quenching of Zn vapor in a hot-wall aerosol flow reactor. *Chemical Engineering Science* 2009;64(5):1095–101.
- [18] Abu Hamed T, Davidson JH, Stolzenburg M. Hydrolysis of evaporated Zn in a hot wall flow reactor. *Journal of Solar Energy Engineering-Transactions of the Asme* 2008;130(4).
- [19] Ernst FO, Tricoli A, Pratsinis SE, Steinfeld A. Co-synthesis of H-2 and ZnO by in-situ Zn aerosol formation and hydrolysis. *Aiche Journal* 2006;52(9):3297–303.
- [20] Weiss RJ, Ly HC, Wegner K, Pratsinis SE, Steinfeld A. H-2 production by Zn hydrolysis in a hot-wall aerosol reactor. *Aiche Journal* 2005;51(7):1966–70.
- [21] Ernst FO, Steinfeld A, Pratsinis SE. Hydrolysis rate of submicron Zn particles for solar H-2 synthesis. *International Journal of Hydrogen Energy* 2009;34(3):1166–75.
- [22] Vishnevetsky I, Epstein M. Production of hydrogen from solar zinc in steam atmosphere. *International Journal of Hydrogen Energy* 2007;32:2791–802.
- [23] Chambon M, Abanades S, Flamant G. Kinetic investigation of hydrogen generation from hydrolysis of SnO and Zn solar nanopowders. *International Journal of Hydrogen Energy* 2009;34(13):5326–36.
- [24] Funke HH, Diaz H, Liang XH, Carney CS, Weimer AW, Li P. Hydrogen generation by hydrolysis of zinc powder aerosol. *International Journal of Hydrogen Energy* 2008;33(4):1127–34.
- [25] Ortega A. The kinetics of solid-state reactions toward consensus – Part I: uncertainties, failures, and successes of conventional methods. *International Journal of Chemical Kinetics* 2001;33(6):343–53.
- [26] Anderson H. On the controversies in Ta kinetics. *Thermochimica Acta* 1992;203:515–8.
- [27] Alimenti GA, Gschaider ME, Bazan JC, Ferreira ML. Theoretical and experimental study of the interaction of O-2 and H₂O with metallic zinc – discussion of the initial step of oxide formation. *Journal of Colloid and Interface Science* 2004;276(1):24–38.
- [28] Graedel TE. Corrosion mechanisms for zinc exposed to the atmosphere. *Journal of the Electrochemical Society* 1989;136(4):C193–203.
- [29] Mattsson E. Corrosion – an electrochemical problem. *Chemtech* 1985;15(4):234–43.
- [30] Zhou L, Rai A, Piekielek N, Ma XF, Zachariah MR. Ion-mobility spectrometry of nickel nanoparticle oxidation kinetics: application to energetic materials. *Journal of Physical Chemistry C* 2008;112(42):16209–18.
- [31] Rai A, Park K, Zhou L, Zachariah MR. Understanding the mechanism of aluminium nanoparticle oxidation. *Combustion Theory and Modelling* 2006;10(5):843–59.
- [32] Ma X, Zachariah MR. Oxidation anisotropy and size-dependent reaction kinetics of zinc nanocrystals. *The Journal of Physical Chemistry C* 2009;113(33):14644–50.
- [33] Kim SH, Mulholland GW, Zachariah MR. Density measurement of size selected multiwalled carbon nanotubes by mobility-mass characterization. *Carbon* 2009;47(5):1297–302.
- [34] Lall AA, Ma X, Guha S, Mulholland GW, Zachariah MR. Online nanoparticle mass measurement by combined aerosol particle mass analyzer and differential mobility analyzer: comparison of theory and measurements. *Aerosol Science and Technology* 2009;43(11):1075–83.
- [35] Smith SM, Schlegel HB. Molecular orbital studies of zinc oxide chemical vapor deposition: gas-phase hydrolysis of diethyl zinc, elimination reactions, and formation of dimers and tetramers. *Chemistry of Materials* 2003;15(1):162–6.